NANO LETTERS

LETTER

pubs.acs.org/NanoLett

Optical Control of Edge Chirality in Graphene

Milan Begliarbekov,[†] Ken-Ichi Sasaki,[‡] Onejae Sul,[§] Eui-Hyeok Yang,[§] and Stefan Strauf*[,†]

[†]Department of Physics and Engineering Physics, Stevens Institute of Technology, Hoboken, New Jersey 07030, United States

[‡]NTT Basic Research Laboratories, Nippon Telegraph and Telephone Corporation, Atsugi, Japan

[§]Department of Mechanical Engineering, Stevens Institute of Technology, Hoboken, New Jersey 07030, United States

Supporting Information

ABSTRACT: We performed optical annealing experiments at the edges of nanopatterned graphene to study the resultant edge reconstruction. The lithographic patterning direction was orthogonal to a zigzag edge. μ-Raman spectroscopy shows an increase in the polarization contrast of the G band as a function of annealing time. Furthermore, transport measurements reveal a 50% increase of the GNR energy gap after optical exposure, consistent with an increased percentage of armchair segments. These results suggest that edge chirality of graphene devices can be optically purified post electron beam lithography, thereby enabling the realization of chiral graphene nanoribbons and heterostructures.

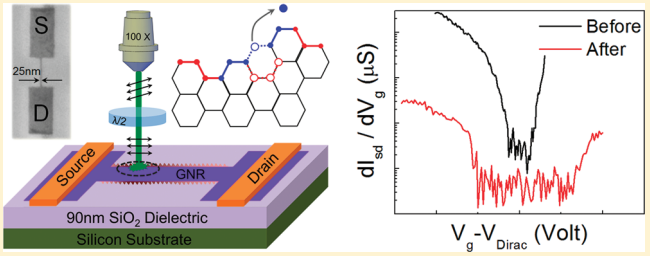

KEYWORDS: Graphene nanoribbons, edge reconstruction, optical annealing, armchair, zigzag, Raman scattering,

Spatially selective bond rearrangement has been a long-standing goal in materials science and chemistry, since it offers the possibility of tailoring the physical properties of molecular species that cannot otherwise be realized via conventional chemical techniques. Site-specific bond alteration has been previously achieved via targeted bond breaking by an STM tip[1] and gas-phase electron attachment.[2] Optically initiated bond rearrangement is of particular interest and was previously demonstrated utilizing precisely tailored femtosecond strong-field laser pulses.[3,4] Here we demonstrate that optically initiated bond rearrangement can be achieved at graphene's edges using selective low-power laser excitation of localized phonons, thereby enabling high-throughput chirality control. In particular, we show that the band gap of lithographically patterned graphene nanoribbons (GNRs) can be increased by 50%, post electron beam lithography, by optically annealing their edges. Consequently, this technique offers novel possibilities for fabricating chiral heterostructures from graphene.

Recently, graphene has been identified as a novel material system for numerous electronic,[5] photonic,[6] and nanomechanical devices.[7] Furthermore, since nanopatterned graphene has attracted a great deal of research attention, an understanding and an ability to control the edge states in nanopatterned graphene devices is of utmost importance since their physical[8] and chemical[9] properties are highly sensitive to edge chirality, which is randomized during conventional manufacturing processes. Unlike bulk graphene, graphene nanoribbons were shown to possess a band gap that is inversely proportional to their width[10,11] and dependent on their edge chirality.[12] While zigzag edges are metallic, armchair edges are semiconducting,[13] and are therefore more desirable for electronic and photonic applications. However, lithographic techniques that are often utilized to pattern GNRs[14,15] typically produce random edges. Ritter et al. recently showed that the gap energy of an armchair GNR of fixed width is significantly reduced if large numbers of zigzag edges are present.[12] Consequently, a method for transforming random and impure armchair edges into high-purity armchair edges is essential for realizing high efficiency graphene p−n junctions,[16,17] which were recently shown to operate at frequencies exceeding 100 GHz,[18,19] as well as other GNR based devices.[20,21]

High-purity zigzag edges were previously obtained using direct electron beam irradiation[14,15] and electron beam lithography.[22] While lithographically defined edges are desirable, the dynamics of the carbon atoms at the edge favors the formation of the zigzag chirality.[15] Consequently, very few armchair edges are typically formed post lithography, thus additional fabrication steps are required. Joule heating inside a transmission electron microscope (TEM)[14] and scanning tunneling microscope (STM) lithography[23] were previously used to form small fractions of armchair edges. In this Letter we experimentally demonstrate a technique utilized to purify armchair edges post electron beam lithography by polarization controlled laser annealing. The technique relies upon the fact that armchair and zigzag edges support different phonon modes that exhibit a 90° phase shift with respect to the polarization of the incident laser beam.[24−26] Consequently, the laser polarization can be adjusted to selectively excite only the zigzag components thereby triggering edge reconstruction at an impure armchair edge, as shown schematically in Figure 1.

Received: August 6, 2011
Revised: October 20, 2011

   dx.doi.org/10.1021/nl2027316 | *Nano Lett.* XXXX, XXX, 000–000

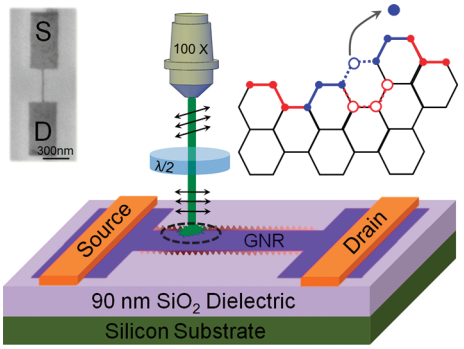

Figure 1. Schematic of the experimental setup used to obtain high-purity armchair edges. A half wave plate is used to rotate the polarization of the laser beam perpendicular to a GNR edge in order to selectively excite the zigzag components which support the TO phonon mode and facilitates edge reconstruction (right inset). The left inset shows an exemplary SEM of a 25 nm GNR used during these experiments.

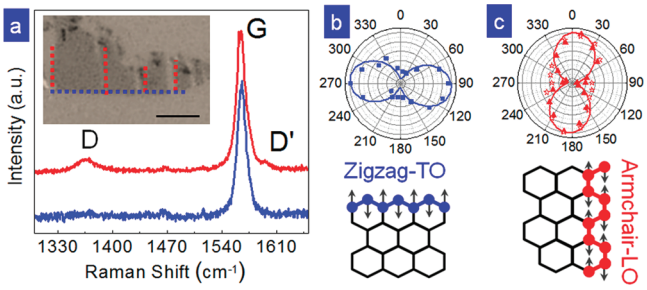

Figure 2. (a) Exemplary Raman spectra at the edges of a graphene flake shown in the inset. The length of the scale bar in the inset is 3 μm. The spectra have been offset for clarity. The polarization dependence of the G band is shown in (b) for the zigzag and in (c) for the armchair edges (triangles). The zigzag edge intensity is fitted by $I_{TO}^{(Z)} \propto \sin^2 \Theta$, while armchair edge intensity is fitted by $I_{LO}^{(A)} \propto \cos^2 \Theta$, where Θ is the angle between the polarization axis of the laser and the edge. The open stars show the polarization dependence of the D band at the armchair edge. The arrows in the diagrams indicate the directions of vibrational motion.

In addition to being technologically relevant, our results also address an open question in the theory of edge stability. While some theories of edge reconstruction predict that zigzag edges should be more stable,[14,15] DFT calculations show that armchair edges are more stable.[27] By selectively exciting both zigzag and armchair edges with two laser polarizations (parallel or perpendicular to the edges, respectively), we show that the zigzag components of an impure armchair edge can be optically annealed resulting in a higher degree of armchair purity, which indicates that zigzag edges are less stable than armchair edges in accordance with the DFT model.

Figure 1 shows a schematic of the experimental setup. The graphene flakes used in these experiments were prepared by micromechanical exfoliation of natural graphite and identified as being monolayer by Raman microscopy.[28] Several flakes with predominantly zigzag edges were identified by the absence of the D-band in the Raman spectrum[29] as well as their characteristic dependence of the G-band intensity on the laser polarization.[24,25,30] Further details of this identification procedure are given elsewhere[24] and described briefly below. After identifying a zigzag edge, 90° cuts were made perpendicular to the edge using e-beam lithography followed by oxygen plasma etching. The 90° angle was chosen so that the resultant edge would be aligned with the armchair crystallographic direction. An exemplary flake used in these experiments is shown in the inset of Figure 2a, with the blue line outlining the zigzag edges and the red line outlining the cut armchair edges.

The chirality of the cut edges was identified post e-beam lithography using polarization resolved μ-Raman spectroscopy. Figure 2a shows exemplary spectra of zigzag and armchair edges. The spectra were obtained by first rotating the sample such that the edge in question is parallel to the laser polarization and then rotating the laser polarization using a half wave plate, thereby interrogating the edge with various polarizations. The angle Θ in panels b and c of Figure 2 is measured between the polarization axis of the incident light and the edge. The armchair edges exhibit both D ($\sim$1350 cm^{-1}) and D′ ($\sim$1610 cm^{-1}) bands, while the zigzag edges do not. The D and D′ bands originate from a doubly resonant scattering process, the boundary conditions for which are only fulfilled by the armchair edges.[31,32] In addition to the presence of the D and D′ bands, the edges can be further confirmed as being armchair by their dependence of the intensity of the G band ($\sim$1580 cm^{-1}) on the polarization of the incident laser beam. This characteristic dependence stems from the asymmetry of the underlying phonon modes that are excited at the edges. At the armchair edge only a parallel (longitudinal) vibration of the optical phonon (LO) mode belonging to the E_{2g} point group is excited, while at the zigzag edge only a perpendicular (transverse) optical phonon (TO) mode is excited.[25] Therefore, the dependence of the intensity of a zigzag edge $I_{TO}^{(Z)}$ varies according to $I_{TO}^{(Z)} \propto \sin^2 \Theta$, while the intensity dependence of the armchair edge $I_{LO}^{(A)}$ varies according to $I_{LO}^{(A)} \propto \cos^2 \Theta$.[24] Panels b and c of Figure 2 show the intensity dependence of the G band on the laser polarization. Since the 90° phase shift of the polarization dependence stems from the different underlying phonon modes that are supported by the armchair and zigzag edges, the phase shift provides an unambiguous signature of edge chirality. The open stars in Figure 2c show the polarization dependence of the D band at the armchair edges. Since the D band can be activated by both armchair edges as well as adsorbed impurities, and rough edges,[32] a smaller polarization contrast, as compared to that of the G band, is observed, as discussed in detail below.

The polarization contrast ($C_P = 1 - I_{min}^{G}/I_{max}^{G}$) of the G band provides further information about edge purity.[24,25] Greater polarization contrast is indicative of higher purity edges, i.e., edges that have a fewer number of segments of the other chirality. The polarization dependence of an armchair edge post e-beam cutting is shown in Figure 3a (blue stars). Although the intensity dependence follows $I_{LO}^{(A)} \propto \cos^2 \Theta$, the polarization contrast is only $C_P^{(A)} = 0.31$. The moderate polarization contrast is indicative of the low purity of the armchair edge. This observation is consistent with previous experiments where it was shown that zigzag edges are preferentially formed during e-beam lithography.[14,15] However, theoretical predictions also reveal that the zigzag edges are unstable.[27] Consequently, they may be transformed into armchair segments.

In order to initiate this transformation, we annealed the zigzag edge by an incident laser (λ = 532 nm) beam focused on the edge using an objective lens with 100-fold magnification and an excitation power of 1.5 mW at the entrance aperture. Figure 3a shows a largely increased polarization contrast of a lithographically cut edge post laser annealing. Figure 3b shows the increase of the polarization contrast as a function of annealing time

dx.doi.org/10.1021/nl2027316 |Nano Lett. XXXX, XXX, 000–000

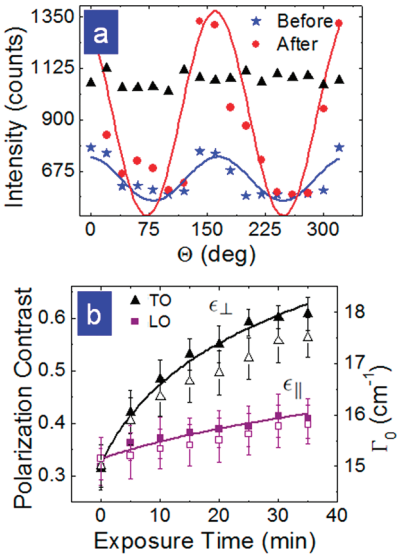

Figure 3. (a) Intensity of the G-band as a function of laser polarization at an e-beam cut edge before (blue stars) and after (red circles) laser annealing with the TO mode. The black triangles are the intensity of the G-band at the interior of the flake. (b) Temporal evolution of the polarization contrast of the G-band during annealing with the LO mode (filled squares) obtained by setting the laser polarization $\varepsilon_\parallel$ to the edge and the TO mode (filled triangles) obtained by setting the laser perpendicular $\varepsilon_\perp$ to the edge. The open symbols correspond to the width of the G mode Γ_0 plotted on the right axis.

displaying a 94% increase ($C_P^{(A)} = 0.6$) after 35 min exposure. The temporal evolution of C_P as well as the width of the G mode Γ_0, as discussed below, was obtained by periodically recording Raman spectra during the course of the exposure. Special care was taken to ensure that the time during the course of which the half wave plate was rotated to its orthogonal configuration (which is necessary in order to ascertain the value of I^G_{min}) was minimized (typically less than 30 s). Furthermore, to verify the mechanism of edge reconstruction, first the laser polarization was set perpendicular to the armchair edge $\varepsilon_\perp$ to excite only the TO phonon mode, which is Raman active at the zigzag edges. Then, the polarization of the incident beam was rotated parallel to a different armchair edge on the same flake $\varepsilon_\parallel$ to excite the LO mode, which is Raman active at the armchair edges, as shown in the inset of Figure 2a. The results show a substantial improvement in the purity of the armchair edge after annealing with the TO phonon mode, while only a moderate increase in the polarization contrast is observed after annealing with the LO mode. In addition to the improved polarization contrast, a broadening of the G mode is observed post laser annealing, as shown in Figure 3b.

In addition, we repeated the above procedure at the zigzag edges of a different flake. In that case a slight improvement of 13% in the polarization contrast was observed; however, neither the width nor the energetic position of the Raman mode was changed (see S1 in the Supporting Information). It should be further pointed out that at the edges of graphene, only the LO mode can undergo the Kohn anomaly,[25] which is a renormalization of the phonon energy via the creation of electron−hole pairs from the phonon mode.[33−35] Since the LO mode is Raman active at the armchair edge, a shift of the phonon energy is not expected at the zigzag edge. These findings are consistent with the fact that additional rearrangement is not expected to occur at a predominantly zigzag edge.

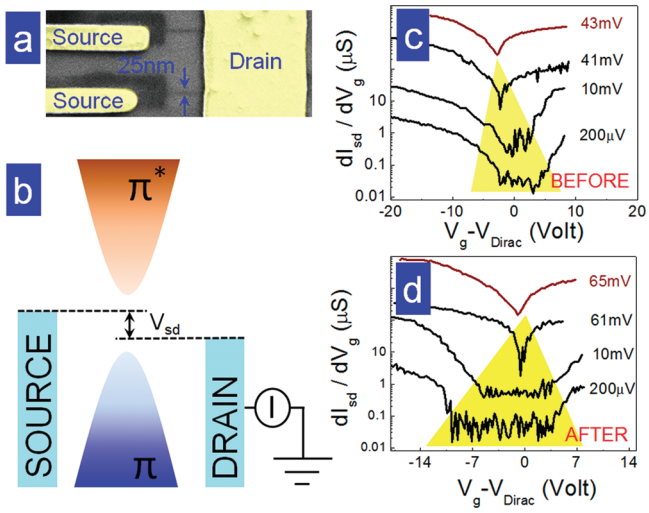

Figure 4. (a) An SEM micrograph of an exemplary 25 nm GNR array used during these experiments. (b) A schematic of the technique for measuring the size of the electronic band gap. Systematically increasing the source−drain bias V_{sd} enlarges the transport window, while varying the backgate voltage V_g displaces the density of states through the transport window. When the size of V_{sd} becomes larger than the electronic band gap, an increase of the minimum conductivity at the Dirac point is observed. Differential current measurements taken at different source−drain biases (c) before and (d) after 45 min of laser annealing.

The broadening of the G mode was previously observed in high-purity armchair edges and originates from a phonon anomaly that takes place at the armchair edge,[25,26] and serves as a further confirmation of greater edge purity. In our samples, a systematic broadening of the width of the G mode, Γ_0, from Γ_0 = 15 to 17.5 cm^{-1} was observed as a function of laser annealing time, indicating a greater purity of armchair edges. Since the greatest improvement in polarization contrast was obtained when the zigzag components were preferentially excited, we conclude that zigzag edges are less stable than armchair edges, in accordance with the DFT model of edge stability.[27] The smaller increase in polarization contrast following annealing with the $\varepsilon_\parallel$ polarization is believed to originate from the fact that the incident laser heats the underlying SiO_2 substrate, which can transfer energy back to the lattice. We further note that in similar experimental conditions Bericaud et al.,[36] utilized the width of the G mode to estimate the optical phonon temperature of the lattice optical emission from the sample to gauge the electron temperature. Using their data as a guide, we expect electron and optical phonon temperatures in our samples to be ∼1900 and 900 K, respectively.

In order to exclude the possibility that the observed polarization dependence of the G and D modes can originate from defects or irregular edges, we annealed the central region (larger than 5 μm from the edge) of a separate graphene flake for 45 min using the same excitation power. The G mode in that interior region exhibited a random 6% variation in intensity but did not show any pronounced intensity dependence on the laser polarization, as shown in Figure 3a. We further note that in previous experiments carried out in an oxygen atmosphere both in the basal plane[37] and at the edges of nonchiral GNRs[38] atmospheric oxygen binding that leads to hole doping resulted in a decrease of Γ_0. Consequently, the systematic increase of Γ_0 suggests that the effects of edge reconstruction are dominant over atmospheric

dx.doi.org/10.1021/nl2027316 |*Nano Lett.* XXXX, XXX, 000–000

oxygen binding, if the patterning direction is chosen to be perpendicular to a zigzag edge.

To further investigate the mechanism for edge reconstruction and to demonstrate its utility, several electrically contacted 25 nm wide GNRs were fabricated, as shown in Figure 4a. Differential transport measurements using standard lock-in techniques were taken before and after laser annealing inside a closed-cycle liquid helium cryostat with a base temperature of 12 K at the sample holder, as shown in panels c and d of Figure 4, respectively. The traces were taken at different source−drain biases V_{sd} in order to measure the size of the electronic gap E_g. For small values of V_{sd}, the conductance through the GNR becomes strongly suppressed for a range of gate biases ΔV_g. Increasing V_{sd} decreases ΔV_g since V_{sd} defines the size of the transport window, as shown schematically in Figure 4b. The source−drain bias at which $\Delta V_g \rightarrow 0$ corresponds to the energy of the electronic transport gap.[11] Conductance traces that are taken at a source−drain bias that is above this value (top curves in panels c and d of Figure 4) display a significantly smaller on/off ratio, which indicates that a finite density of states is present in the transport window at all times. Prior to laser annealing a 41 meV electronic gap was measured, as seen in Figure 4c. The gap energy was increased by 50% to 61 meV, as shown in Figure 4d following 45 min of laser annealing, with the laser polarization rotated perpendicular to the GNR in order to excite the TO mode at the zigzag edges. In addition to an increased electronic gap E_g the increase in ΔV_g before and after annealing points to an increased mobility gap ΔE_m, which originates from the presence of a finite disorder potential at the edges of the GNR.[39,40] The size of this mobility gap can be estimated from $\Delta E_m \approx \hbar v_F((2\pi C_g \Delta V_g)/|e|)^{1/2}$, where $v_F = 1.1 \times 10^6$ m s^{-1} is the Fermi velocity and C_g is the back-gate capacitance per square micrometer, obtained from finite element analysis to be 690 aF/μm^2 in ref 35. Prior to laser annealing a $\Delta V_g = 8.6$ V, corresponding to $\Delta E_m \approx 318$ meV was measured, while after annealing ΔV_g increased to 11.3 V, corresponding to $\Delta E_m \approx 364$ meV. While the electronic gap E_g was increased by 50% post laser annealing, the disorder related mobility gap was only increased by 14%. Although E_g is affected by both edge chirality and disorder, the substantially smaller increase in ΔE_m, which originates purely from disorder, points to the fact that a greater number of armchair segments are created post laser annealing in agreement with the Raman signatures.

To rule out effects of width variation post laser annealing as an alternate cause for the increased electronic gap, scanning electron photomicorgraphs of several GNRs were taken before and after laser irradiation of different GNR devices. We note that the devices used for the optical and transport measurements were not imaged prior to measurement since direct electron beam irradiation can randomize the edges as well as introduce other defects. No width variation after 45 min laser irradiation was observed within the ±1.5 nm resolution of the scanning electron photomicorgraph. It is also known that 12 h of continuous laser exposure is necessary before damage can be observed.[41] To further account for the possible variation in the ribbon width that is not resolved in the scanning electron photomicorgraphs we note that decreasing the ribbon width would introduce a greater confinement gap of $\Delta E_{con} = \gamma\pi a_{C-C}/w$, where $\gamma = 2.8$ eV is the nearest neighbor hopping energy and $a_{C-C} = 0.142$ nm is the carbon−carbon separation. On the basis of these parameters, one can estimate that the possible 1.5 nm variation in GNR width can only increase the resultant band gap by 6% and thus cannot account for the observed 50% increase in E_g.

Therefore, the increase in electronic band gap can be attributed to the presence of a larger amount of armchair segments, which, in agreement with previous tunneling spectroscopy experiments,[12] results in a larger electronic band gap energy at fixed GNR width as compared to zigzag or rough edges. This result, combined with the increase in the Raman polarization contrast indicates that the polarization controlled laser annealing process creates an overall larger amount of armchair segments than random defects, i.e., an optical control of edge chirality.

Direct imaging techniques of the GNR edges were not employed during these experiments since it was previously shown that electron beam irradiation inside a TEM can lead to significant edge reconstruction of free-standing graphene, which would alter the effect of the optical control of edge chirality during observation.[14,18] While the local density of states at the edges of unzipped carbon nanotubes was recently successfully imaged using STM,[42] the STM technique requires that the GNR is placed on a conductive substrate, on which the method of edge reconstruction has not yet been investigated. Therefore, polarization resolved μ-Raman spectroscopy combined with electron transport provides unambiguous signatures of edge chirality and purity, which are compatible with nanostructured graphene devices located on nonconducting dielectrics necessary for electronic device applications.

Finally we note that the ratio of the minimum to maximum intensity of the G band corresponds to the ratio of the zigzag part to the armchair.[25] We can thus estimate that the percentage of armchair edges increases from 60 to 75% post our annealing procedure, as discussed in the Supporting Information. It is interesting to note that a rather moderate increase of edge purity results in a substantial increase ~50% in the electronic band gap. These results, are consistent with the measurements of Ritter and Lyding[12] who showed that the value of the band gap scales superlinearly with edge purity. Consequently, if coherent control of edge chirality can be achieved, which may require a more complex shape of laser light (phase, intensity, etc), the electronic band gap of graphene may be purified even more thereby rendering graphene suitable for numerous electronic and photonic applications.

In summary, we have shown that laser annealing of low-purity armchair edges post e-beam lithography leads to edge reconstruction and an increased electronic band gap. Three optical and a transport signature have been used to confirm the purification of the armchair edge. The best results were obtained if the polarization of the laser was set to selectively excite only the zigzag edges, which also verifies theoretical predictions of the relative metastability of zigzag edges. Optical control of edge chirality offers novel possibilities for fabricating devices with different edges or alternating edge types, such as Z-shaped heterojunctions which were predicted to rectify current[43] but have not yet been experimentally realized.

■ ASSOCIATED CONTENT

Supporting Information. Details on effects of annealing at zigzag edges and estimating edge purity. This material is available free of charge via the Internet at http://pubs.acs.org.

■ AUTHOR INFORMATION

Corresponding Author
*E-mail: strauf@stevens.edu.

dx.doi.org/10.1021/nl2027316 |*Nano Lett.* XXXX, XXX, 000–000

■ ACKNOWLEDGMENT

We thank Michael Crommie and Michael Chabinyc for fruitful discussions. Partial financial support was provided by the National Science Foundation, award ECCS-1104870. We also thank the Center for Functional Nanomaterials of the Brookhaven National Laboratory, Contract DE-AC02-98CH10886, for the use of their clean room facilities.

■ REFERENCES

(1) Dujardin, G.; Walkup, R. E.; Avouris, P. *Science* **1992**, *255*, 1232–1235.
(2) Baccarelli, I.; Gianturco, F. A.; Grandi, A.; Sanna, N.; Lucchese, R. R.; Bald, I.; Kopyra, J.; Illenberger, E. *J. Am. Chem. Soc.* **2007**, *129*, 6269–6277.
(3) Levis, R. J.; Menkir, G. M.; Rabitz, H. *Science* **2001**, *292*, 709–713.
(4) Assion, A.; Baumert, T.; Bergt, M.; Brixner, T.; Kiefer, B.; Seyfried, V.; Strehle, M.; Gerbe, G. *Science* **1998**, *282*, 919–922.
(5) Geim, A. K. *Science* **2009**, *324*, 1530–1534.
(6) Bonaccorso, F.; Sun, Z.; Hasan, T.; Ferrari, A. C. *Nat. Photonics* **2010**, *4*, 611–622.
(7) Chen, C.; Rosenblatt, S.; Bolotin, K. I.; Kalb, W.; Kim, P.; Kymissis, I.; Stormer, H. L.; Heinz, T. F.; Hone, J. *Nat. Nanotechnol.* **2009**, *4*, 861–867.
(8) Son, Y.-W.; Cohen, M. L.; Louie, S. G. *Nature* **2006**, *444*, 347–349.
(9) en Jiang, D.; Sumpter, B. G.; Dai, S. *J. Chem. Phys.* **2007**, *126*, 134701.
(10) Barone, V.; Hod, O.; E, S. G. *Nano Lett.* **2006**, *6*, 2748–2754.
(11) Han, M. Y.; Ozyilmaz, B.; Zhang, Y.; Kim, P. *Phys. Rev. Lett.* **2007**, *98*, 206805.
(12) Ritter, K. A.; Lyding, J. W. *Nat. Mater.* **2009**, *8*, 235–242.
(13) Son, Y.-W.; Cohen, M. L.; Louie, S. G. *Phys. Rev. Lett.* **2006**, *97*, 216803.
(14) Jia, X.; Hofmann, M.; Meunier, V.; Sumpter, B. G.; Campos-Delgado, J.; Romo-Herrera, J. M.; Son, H.; Hsieh, Y.-P.; Reina, A.; Kong, J.; Terrones, M.; Dresselhaus, M. S. *Science* **2009**, *323*, 1701–1705.
(15) Girit, C. O.; Meyer, J. C.; Erni, R.; Rossell, M. D.; Kisielowski, C.; Yang, L.; Park, C.-H.; Crommie, M. F.; Cohen, M. L.; Louie, S. G.; Zettl, A. *Science* **2009**, *323*, 1705–1708.
(16) Huard, B.; Sulpizio, J. A.; Stander, N.; Todd, K.; Yang, B.; Goldhaber-Gordon, D. *Phys. Rev. Lett.* **2007**, *98*, 236803.
(17) Begliarbekov, M.; Sul, O.; Ai, N.; Yang, E.-H.; Strauf, S. *Appl. Phys. Lett.* **2010**, *97*, 122106.
(18) Lin, Y. M.; Dimitrakopoulos, C.; Jenkins, K. A.; Farmer, D. B.; Chiu, H. Y.; Grill, A.; Avouris, P. *Science* **2010**, *327*, 662.
(19) Liao, L.; Lin, Y.-C.; Bao, M.; Cheng, R.; Bai, J.; Liu, Y.; Qu, Y.; Wang, K. L.; Huang, Y.; Duan, X. *Nature* **2010**, *467*, 305–308.
(20) Begliarbekov, M.; Sul, O.; Santanello, J.; Ai, N.; Zhang, X.; Yang, E.; Strauf, S. *Nano Lett.* **2011**, *11*, 1254.
(21) Begliarbekov, M.; Strauf, S.; Search, C. P. *Nanotechnology* **2011**, *22*, 165203.
(22) Krauss, B.; Nemes-Incze, P.; Skakalova, V.; Biro, L. P.; von Klitzing, K.; Smet, J. H. *Nano Lett.* **2010**, *10*, 4544–4548.
(23) Tapaszto, L.; Dobrik, G.; Lambin, P.; Biro, L. P. *Nat. Nanotechnol.* **2008**, *3*, 397–401.
(24) Begliarbekov, M.; Sul, O.; Kalliakos, S.; Yang, E.-H.; Strauf, S. *Appl. Phys. Lett.* **2010**, *97*, 031908.
(25) Sasaki, K.; Saito, R.; Wakabayashi, K.; Enoki, T. *J. Phys. Soc. Jpn.* **2010**, *79*, 044603.
(26) Zhang, W.; Li, L. J. *ACS Nano* **2011**, *5*, 3347–3353.
(27) Koskinen, P.; Malola, S.; Hakkinen, H. *Phys. Rev. Lett.* **2008**, *101*, 115502.
(28) Ferrari, A. C.; Meyer, J. C.; Scardaci, V.; Casiraghi, C.; Lazzeri, M.; Mauri, F.; Piscanec, S.; Jiang, D.; Novoselov, K. S.; Roth, S.; Geim, A. K. *Phys. Rev. Lett.* **2006**, *97*, 187401.
(29) You, Y.; Ni, Z. H.; Yu, T.; Shen, Z. X. *Appl. Phys. Lett.* **2008**, *93*, 163112.
(30) Cong, C.; Yu, T.; Wang, H. *ACS Nano* **2010**, *4*, 3175–3180.
(31) Cancado, L. G.; Pimenta, M. A.; Neves, B. R. A.; Dantas, M. S. S.; Jorio, A. *Phys. Rev. Lett.* **2004**, *93*, 247401.
(32) Pimenta, M.; Dresselhaus, G.; Dresselhaus, M.; Cancado, L.; Jorio, A.; Saito, R. *Phys. Chem. Chem. Phys.* **2007**, *9*, 1276–1290.
(33) Lazzeri, M.; Mauri, F. *Phys. Rev. Lett.* **2006**, *97*, 266407.
(34) Ando, T. *J. Phys. Soc. Jpn.* **1996**, *75*, 124701.
(35) Yan, J.; Zhang, Y.; Kim, P.; Pinczuk, A. *Phys. Rev. Lett.* **2007**, *98*, 166802.
(36) Berciaud, S.; Han, M. Y.; Mak, K. F.; Brus, L. E.; Kim, P.; Heinz, T. F. *Phys. Rev. Lett.* **2010**, *104*, 227401.
(37) Ryu, S.; Liu, L.; Berciaud, S.; Yu, Y.-J.; Liu, H.; Kim, P.; Flynn, G. W.; Brus, L. E. *Nano Lett.* **2010**, *10*, 4944.
(38) Ryu, S.; Maultzsch, J.; Han, M. Y.; Kim, P.; Brus, L. E. *ACS Nano* **2011**, *5*, 4123.
(39) Molitor, F.; Stampfer, C.; Guttinger, J.; Jacobsen, A.; Ihn, T.; Enssli, K. *Semicond. Sci. Technol.* **2010**, *25*, 034002.
(40) Han, M. Y.; Brant, J. C.; Kim, P. *Phys. Rev. Lett.* **2010**, *104*, 056801.
(41) Krauss, B.; Lohmann, T.; Chae, D.-H.; Haluska, M.; von Klitzing, K.; Smet, J. H. *Phys. Rev. B* **2009**, *79*, 165428.
(42) Tao, C.; Jiao, L.; Yazyev, O. V.; Chen, Y.-C.; Feng, J.; Zhang, X.; Capaz, R. B.; Tour, J. M.; Zettl, A.; Louie, S. G.; Dai, H.; Crommie, M. F. *Nat. Phys.* **2011**, *7*, 616.
(43) Wang, Z. F.; Li, Q.; Shi, Q. W.; Wang, X.; Hou, J. G.; Zheng, H.; Chen, J. *Appl. Phys. Lett.* **2008**, *92*, 133119.